244 (2025) 213469

Contents lists available at ScienceDirect

Geoenergy Science and Engineering

journal homepage: www.sciencedirect.com/journal/geoenergy-science-and-engineering

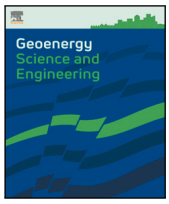

A three-phase dispersion profile model for stratified pipe flow: Effects of gas bubbles on the distribution of oil and water droplets

R. Skartlien [a,*], J. Nossen [a], G.W. Johnson [b], T.K. Kjeldby [b]

[a] Institute for Energy Technology, Department for Flow Technology, Instituttveien 8, Kjeller, 2007, Norway
[b] Equinor ASA, Hydroveien 79, Porsgrunn, 3948, Norway

ARTICLE INFO

Keywords:
Three phase flow modelling
Dispersion profiles
Turbulence modulation
Entrainment
Hindered settling

ABSTRACT

A three-phase dispersion profile model for stratified gas/oil/water pipe flow was developed. The main goal was to incorporate the effects of gas bubbles on the cross-sectional distribution of oil and water droplets in the continuous liquids. Gas bubbles entrain from the gas layer above the oil/water layers and modify the oil and water dispersion profiles in several different ways. Increased hindered settling due to gas bubbles, reduction of the effective background mixing density that affects buoyancy, turbulence suppression due to droplets and bubbles and finally reduction of oil and water droplet entrainment rate due to area blocking by gas bubbles at the oil/water interface. All three dispersion profiles were modelled consistently with respect to their mutual coupling. The tuned model qualitatively reproduced the shapes and magnitude of the volume fraction profile data obtained from X-ray measurements. Several areas were identified where more fundamental experimental research would be needed.

1. Introduction

A long standing problem for flow simulators has been uncertain prediction of the amount of oil and water dispersions mixed into the continuous fluid layers when gas bubbles are entrained into these layers. In the current work, we focus on models for cross sectional oil and water dispersion profiles that incorporate the influence of entrained gas bubbles from the overlying gas layer. The model governs time- or ensemble averaged dispersion profiles in statistically stationary near horizontal stratified/wavy three-layer flow, with focus on the dispersion profiles in the two adjacent oil and water layers (Fig. 1). It is plausible that the main effects of gas bubbles are altered gravitational settling due to lowered average mass density in the background fluid, increased hindered settling, modified turbulence levels that affect the droplet diffusion coefficients, and altered boundary conditions at the large scale oil/water interface (O/W LSI). These ingredients were incorporated into our model by invoking a series of assumptions that are discussed in Section 2.

Substantial experimental efforts have been made regarding the behaviour of stratified oil/water two-phase flow (*e.g.*, Lovick and Angeli, 2004; Ioannou et al., 2005; Brauner and Ullmann, 2002; Paolinelli, 2020; Ngan et al., 2009; Amundsen, 2011; Elseth, 2001). A recent comprehensive review for oil/water flow is found in Ahmed and John (2018). The volume of literature is less extensive for water/oil/gas flow. A recent review of gas–liquid–liquid three-phase flow patterns, pressure drop, and liquid holdup in pipelines is due to Yaqub et al. (2020). Flow regime maps and profile data for three phase flow can be found in Khor (1998) and Hewitt (2005), and Taitel et al. (1995) calculated gas/oil/water holdups for stratified three phase flow. Sassi et al. (2020) performed experiments on gas–liquid–solid three phase flow. Droplet sizes and size distributions have been measured with varying techniques for oil/water flow by *e.g.*, Sajjadi et al. (2002), Angeli and Hewitt (2000), Kjølaas et al. (2022), while phase inversion studies in oil/water pipe flow were performed by *e.g.*, Brauner and Ullmann (2002), Ngan et al. (2009), Ioannou et al. (2005), Piela et al. (2008). Cross sectional turbulence and velocity profiles were measured in oil/water flow by *e.g.*, Amundsen (2011) and Elseth (2001).

Of recent profile modelling for oil/water dispersions in stratified pipe flow, we note the works of Valle (2000), Amundsen (2011), Kjølaas et al. (2022). These works also provided new datasets for volume fraction profiles. Evripidou et al. (2022) developed a model for the transition of oil/water dispersion flow along a pipe, and Smith et al. (2015) developed a point model for stationary gas/oil and water/oil pipe flow. We are not aware of previous modelling efforts for cross sectional oil and water dispersion profiles that incorporate the influence of entrained gas bubbles from an overlying gas layer, and the goal with the current work was to construct such a model.

The largest modelling uncertainties, in addition to the influence from bubbles, are associated with the entrainment and deposition rates

* Corresponding author.
E-mail address: roar.skartlien@ife.no (R. Skartlien).

https://doi.org/10.1016/j.geoen.2024.213469
Received 26 June 2024; Received in revised form 15 October 2024; Accepted 2 November 2024
Available online 15 November 2024

of droplets at large scale interfaces (LSI), droplet size distributions in dense and opaque turbulent emulsions, turbulence and wall friction modification due to droplets and bubbles, deviation of droplet and bubble diffusion coefficients from the single phase eddy diffusivity. Altered turbulence, hindered settling and buoyancy are the main effects from bubbles. A broader overview of the relatively complex physical effects in dispersed flow is given next, which underlines the challenges and uncertainties that are associated to dispersion modelling.

Entrainment from the LSI and deposition onto the LSI is influenced by the presence of surface active hydrocarbons and acids in oil that alter interfacial tension and interfacial stability and breakup dynamics. Surface active molecules also influence the droplet and gas bubble size distribution through increased breakup and reduced coalescence rates that will skew the size distribution to smaller diameters relative to clean fluids (Skartlien et al., 2012, 2013). Direct measurement of droplet and bubble sizes (in particular in opaque oil) remains a challenge, and hence input to the modelling of settling velocities is limited.

Is is clear that turbulence modulation in the presence of high volume fractions of droplets and/or bubbles is potentially very important, with implications for wall and interfacial friction, and pressure drop along the pipe. Turbulence profiles have indeed been measured in dispersion flow (*e.g.*, Elseth, 2001), but the nature and level of turbulence modulation in these flows have not been clarified to any extent. For more ideal cases of solids in gas or liquid, the degree of turbulence modulation has been measured to be quite substantial relative to single phase flow (Gore and Crowe, 1989; Saber et al., 2015; Hetsroni, 1989; Kenning and Crowe, 1997). For particle sizes that lie between the Kolmogorov scale and a small fraction of the integral length scale there is turbulence suppression due to enhanced dissipation (Kenning and Crowe, 1997). There is turbulence enhancement for larger particles due to vortex shedding (Hetsroni, 1989), but this is less likely for droplets and bubbles as the sizes are limited by turbulent breakup. One would therefore expect only turbulence suppression in dispersions, as discussed by Skartlien et al. (2023). Further experimental efforts are encouraged to be able to clarify these mechanisms. For droplets larger than the Kolmogorov scale, the vortex structures (tubes and sheets) can be directly modified and possibly break up by hydrodynamic interaction with droplets and bubbles, and the flow of turbulence energy to smaller scales (the cascade) is now enhanced, resulting in increased dissipation rates. Increased dissipation may also occur more directly in the small scale velocity gradients between droplets (Kenning and Crowe, 1997).

Modified wall friction has usually been accounted for in earlier work by invoking an emulsion or dispersion viscosity (*e.g.*, Pal and Rhodes, 1985; Ngan et al., 2009). However, emulsion viscosity is an "effective fluid" concept that is physically meaningful only when the droplet sizes are *smaller* than the smallest turbulence length scale (the Kolmogorov scale), so that the flow field is laminar on the droplet scale, and the only flow line disturbances are due to the presence of the droplets. The net wall friction and hence the pressure drop along the pipe is likely to be affected by both direct turbulence modulation in the bulk flow that alters the turbulent momentum flux to the walls (turbulent shear stress), and increased effective emulsion viscosity in the viscous sublayer when small diameter droplets or bubbles reside there. For large dispersion volume fraction, turbulence suppression may be strong so that the flow has a more laminar character where the emulsion viscosity appears to play a larger role with maximum friction and pressure drop near the inversion point (*e.g.*, Angeli and Hewitt, 1999; Ioannou et al., 2005).

The diffusion coefficient of droplets, bubbles or particles is usually taken to be the turbulent eddy diffusivity in the dispersion-free carrier fluid, which is proportional to the friction velocity (characteristic turbulence fluctuation velocity) and the hydraulic diameter (or thickness) of the liquid layer in question. An important mechanism that will affect the diffusion coefficient is preferential concentration where the particles migrate away from vortex cores and accumulate in convergence zones (*e.g.*, Eaton and Fessler, 1994; Reeks, 2014; Bragg et al., 2015). It is therefore reason to believe that the diffusivity is influenced by the structure of the turbulence in relation to droplet size and inertia, not only turbulence magnitude. For large inertial droplets is gas, the droplet motion is only weakly perturbed by the turbulent gas motion, and the eddy diffusivity is less relevant, and the droplet profile is instead controlled by the kinetic energy distribution of the droplets (Skartlien, 2009).

For dense emulsions, the droplets interact hydrodynamically, and hindered settling between the emulsion droplets is important (*e.g.*, Richardson and Zaki, 1954). It is reasonable to expect that the addition of gas bubbles reduces the settling rate of the dispersion droplets by increasing the hindrance effect even more, and we therefore incorporated such hindered settling corrections to the gravitational settling rate. The role of turbulence on the average settling velocity has been explored to some extent (Mei, 1994; Bragg et al., 2021), but this effect has often been ignored.

With these complexities in mind, the motto was to generate a simplified "first order", cross sectional 1D dispersion model that could account for the effects of bubbles in the liquid layers. The three dispersion profiles (oil and water droplets and gas bubbles) were formulated in terms of three coupled first order diffusion equations. The volume fraction profile of one dispersed phase is sensitive to buoyancy alteration, enhanced hindered settling effects, and turbulence suppression induced by the local volume fraction of the other phase. These couplings result in a non-linear system to be solved by iteration. First, we describe the ingredients in the model before we compare the results to the measured volume fraction profiles obtained by an X-ray instrument. Then we provide a discussion of model uncertainties before the conclusions are drawn.

2. Three-phase dispersion model

2.1. General form of the profile model

Four types of dispersion profile scenarios occur simultaneously for adjacent oil and water layers as shown in Fig. 1, with (1) Oil droplets in a background of continuous water and gas bubbles (blue layer in the figure), (2) Water droplets in a background of continuous oil and gas bubbles (brown layer), (3) Gas bubbles in a background of continuous water and oil droplets (blue layer), and (4) Gas bubbles in a background of continuous oil and water droplets (brown layer). We assumed vertical variation of the dispersion profiles only, which is reasonable for flows that are far from annular so that horizontal cross sectional gradients can be ignored. For the most simplified modelling approach for stationary stratified flow, one assumes approximate mass flux balance between gravitational settling (or creaming) and turbulent diffusion in the time averaged sense, provided the net mass flux is zero on the boundaries of the layer in question. We assumed that any of the three dispersions "i" (bubbles, oil and water droplets) obeys the standard first order diffusion equation in a continuous phase background "c" that also contains an additional dispersion "a",

$$\Gamma(\varphi_c, \varphi_a, \varphi_i)\partial_y \varphi_i + v_s(\varphi_c, \varphi_a, \varphi_i)\varphi_i = 0, \tag{1}$$

where the generalized diffusion coefficient Γ and settling velocity v_s are functions of the three volume fractions, and the coordinate y is in the vertical direction perpendicular to the interfaces. It should be noted that we do not account for complete droplet and bubble size distributions, but rather model the settling velocity and turbulence modulation for the diffusion coefficient based on an estimated mean size of the droplets or bubbles. This choice was made to reduce the level of complexity of the model.

For each layer, there will be two coupled equations, one for the droplets and one for the gas bubbles. Furthermore, these will be coupled to two additional equations for the second layer, through the interfacial boundary condition between the oil and water layers (marked

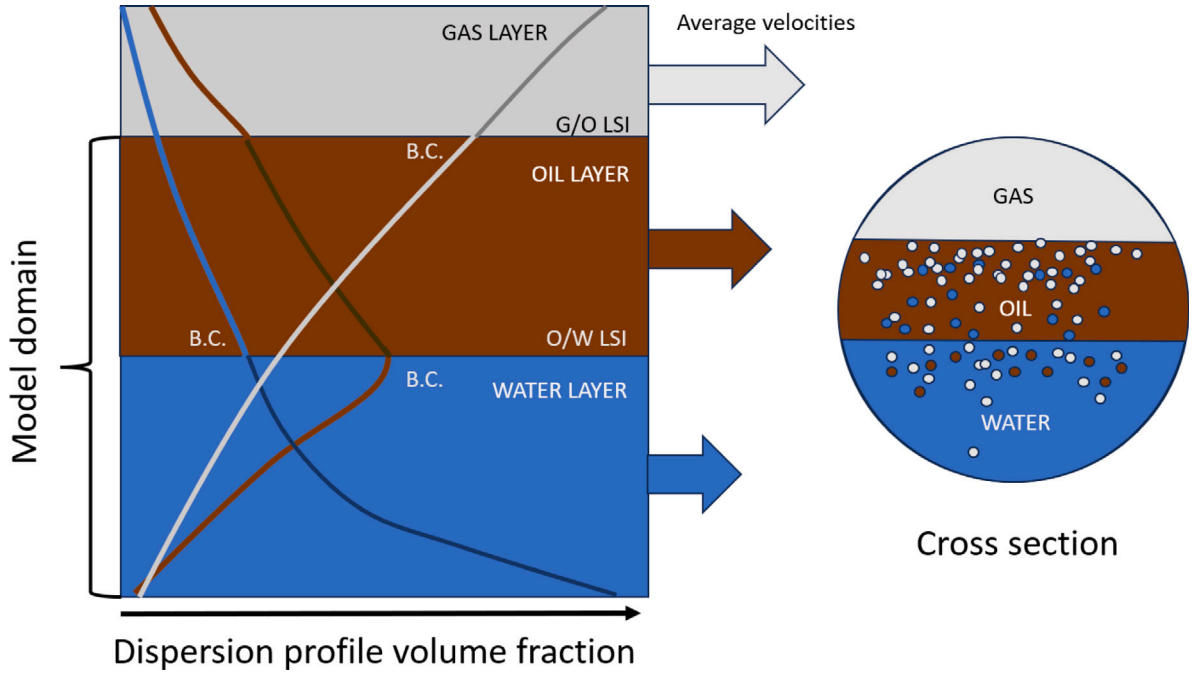

Fig. 1. *Left:* The layered stratified flow structure and dispersion volume fraction profiles are shown with oil droplets in the water layer (brown), and water droplets in oil (blue), and gas bubbles (grey). The darker colours show the continuous phase volume fractions with dark blue in the water layer, dark brown in the oil layer, and dark grey in the gas layer. The two large scale interfaces (LSI) are marked, together with the three boundary conditions for the volume fraction profiles (B.C.). There are two diffusion equations for each layer, one for droplets and one for bubbles. These equations are coupled via the O/W LSI boundary conditions (B.C.), with the influence of gas blocking. The LSI's are in general wavy and/or agitated by turbulence and the figure represents a time averaged view. The relative flow velocity magnitudes are indicated with arrows. *Right:* The corresponding pipe cross section, with droplets and bubbles distributed through the liquid layers (oil and water droplets in gas are not shown here).

O/W LSI in the figure). We do not consider droplets in the gas layer (grey layer in Fig. 1) in this work. A system of this type was solved using numerical integration for each equation with a fourth order Runge–Kutta integrator (RK4), in combination with an "outer" iteration loop for coupling between the four equations. From a mathematical point of view, these iterations were needed since the coefficients in the equation above depends on the solution from the other equations.

2.2. Runge–Kutta integration with iterations

In general, the gas bubble and droplet volume fractions are varying over the cross section, and hence the buoyancy effect and turbulence modulation will also vary in the cross section, and the coupled equations have to be integrated in this context. This constitutes a highly non-linear set of equations with variable coefficients. The diffusion equation for dispersion "i" can in general be written as the first order differential equation

$$\partial_y \varphi_i = -\frac{v_s(\varphi_c, \varphi_a, \varphi_i)}{\Gamma(\varphi_c, \varphi_a, \varphi_i)} \varphi_i \equiv F(\varphi_c, \varphi_a, \varphi_i, y). \tag{2}$$

This can be integrated to obtain $\varphi_i(y)$, and we use the "classical" fourth order Runge–Kutta (RK4) method which is accurate to fourth order in Δy. One must integrate each equation for each phase successively, and substitute the integrated variable φ_i into the next equation to be integrated. This must be repeated in the following iteration loop until convergence is obtained,

1. $\partial_y \varphi_g = F(\varphi_o, \varphi_w, \varphi_g, y)$ gas bubbles in oil layer, given $\varphi_{g,0}$
2. $\partial_y \varphi_w = F(\varphi_o, \varphi_g, \varphi_w, y)$ water droplets in oil layer, given $\varphi_{w,0} = \varphi_{inv}(1 - b\varphi_{g,o/w})$
3. $\partial_y \varphi_g = F(\varphi_w, \varphi_o, \varphi_g, y)$ gas bubbles in water layer, given $\varphi_{g,o/w}$
4. $\partial_y \varphi_o = F(\varphi_w, \varphi_g, \varphi_o, y)$ oil droplets in water layer, given $\varphi_{o,0} = 1 - \varphi_{w,0} - \varphi_{g,o/w}$.

The quantities on the right hand side are the corresponding interfacial boundary values that will be discussed later. Suitable starting values for the profiles must be chosen to avoid divergence, either exponential solutions in y or simply constants at the expense of a few more iterations. To avoid oscillations and to obtain faster convergence rates, a relaxation weight $1 - exp(i/(0.1N_i))$ was introduced as a scaling on the water droplet boundary value $\phi_{w,0}$. Here, i is the iteration number $i \in [1, N_i]$, N_i is the total number of iterations, and the weight approaches 1.0 relatively quickly due to the small relaxation factor of 0.1.

2.3. Settling velocity

The settling velocity is controlled by the droplet or bubble size, hindered settling effects for high volume fraction, and the density of the background fluid that the droplet or bubble resides in. These effects will be discussed next.

2.3.1. Dilute limit of the settling velocity

During settling, the internal circulation in a droplet or bubble depends on the viscosity ratio between the surrounding fluid and the droplet or bubble. However, surfactant-laden or "contaminated" fluids are the norm for hydrocarbon transport where the oil contains indigenous surfactant. The interfacial mobility is then reduced, and the viscosity ratio plays a smaller role. Then for sufficiently small droplets or bubbles that remain close to spherical, the single droplet/bubble settling velocity V_∞ can be estimated using standard drag formulae. To accommodate finite but small Reynolds numbers for a viscous sphere, we adopt the power law (Amundsen, 2011)

$$C_D = \frac{18.5}{Re_p^{0.6}}, \tag{3}$$

which is close to the model of Feng and Michaelides (2001). For very small droplet Reynolds numbers $Re_p = V_\infty d\rho/\mu$, the drag coefficient is close to the Stokes value of $C_D = 24/Re_p$. The chosen power law allows

for an explicit formula for the settling velocity and for a single spherical droplet or bubble of diameter $\overline{d}$,

$$V_\infty = Sgn(\Delta\rho)\left[\frac{4\ g\cos(\theta)\overline{d}|\Delta\rho|}{3\rho C_D}\right]^{1/2} \approx 0.153\frac{\overline{d}^{1.142}(g\cos\theta\Delta\rho)^{0.714}}{\rho_c^{0.286}\mu_c^{0.428}}Sgn(\Delta\rho), \tag{4}$$

where μ_c is the continuous fluid dynamic viscosity, and the density difference $\Delta\rho = \rho_d - \rho_c$ is between the droplet mass density ρ_d and the continuous fluid mass density ρ_c. We use a sign convention such that a positive density difference corresponds to positive settling velocity downwards in the negative y-direction, in the direction of gravity. Sgn is the sign function. θ is the inclination angle of the pipe.

For the maximum stable droplet size in turbulence, we use the classical model by Hinze (1955),

$$d_{\max} = 0.725\left(\frac{\sigma_{ow}}{\rho_c}\right)^{0.6}\varepsilon_{\text{turb}}^{-0.4}, \tag{5}$$

which is appropriate for breakup by turbulent kinetic energy against the oil/water interfacial tension σ_{ow}, assuming that the energy spent on deformation of the droplet is small in comparison. This is the case for relatively low oil viscosity, and obviously the case for gas bubbles, but not necessarily so for viscous oils. For the current oil, we found that the interfacial energy was larger than the viscous work required for breakup, and the Hinze relation was adequate. The settling velocity $V_\infty = V_\infty(\overline{d})$ of the average droplet size $\overline{d}$ is taken to represent a characteristic settling velocity in the dispersion. For a Rosin-Rammler size distribution, the average diameter is $\overline{d} = 0.556 d_{\max}$. The turbulent kinetic energy at the droplet diameter size scale appears in the Hinze formula in terms of the dissipation rate in the fluid, $\varepsilon_{\text{turb}}$. It was estimated as the mean rate of energy dissipation

$$\varepsilon_{\text{turb}} = \left|\frac{\mathrm{dP}}{\mathrm{dz}}\right| U_{layer}/\rho_{mix}, \tag{6}$$

in terms of the pressure gradient, average layer velocity, and the layer mixture density. However, turbulence is modified in the presence of a dispersion, and the turbulent kinetic energy at the droplet scale is also modified. Suppression of total turbulent kinetic energy is most likely (Skartlien et al., 2023), but the change of turbulent kinetic energy at the droplet scale remains uncertain. Due to these uncertainties, it is reasonable to adopt the scaled Hinze form

$$\overline{d} = 0.4 f_d\left(\frac{\sigma_{ow}}{\rho_c}\right)^{0.6}\varepsilon_{\text{turb}}^{-0.4}, \tag{7}$$

where f_d is a tuning factor that have different values for droplets and bubbles. These values were obtained by fitting the modelled profiles to the data. A more direct measure of the local turbulence levels could have been used for transparent fluids to estimate the local dissipation rate (and turbulence modulation), rather than resorting to the pressure gradient for estimation of an average dissipation rate. Measurements of turbulence profiles are however not possible for opaque/crude oil using standard optical approaches.

Breakup and coalescence influence the droplet size distribution, and may affect the average droplet size, not only breakup as modelled by the Hinze-relation. Since the tuned factors vary over dispersion type, we suspect that the mean size estimated from the Hinze-model does not reflect the balance between coalescence and breakup. Furthermore, the mixed dispersion (bubbles and droplets) introduces an extra uncertainty due to increased mutual hydrodynamic interaction in the dispersion (drop and bubble collisions) that may affect breakup and coalescence rates. One of the most important experimental quantities that could be obtained in this context is the droplet and bubble size distributions in mixed dispersions.

2.3.2. Hindered settling with added gas bubbles

For hindered settling in a dense dispersion, a commonly used strategy is to model the settling velocity by

$$v_s = V_\infty(1-\varphi)^n. \tag{8}$$

For solids, the exponent n is a function of the particle Reynolds number (*e.g.*, Richardson and Zaki, 1954). According to the oil/water investigations of Amundsen (2011), $n \simeq 3$, which for the case of solids would correspond to a particle Reynolds number between 10 and 100. For a particle Reynolds number close to unity, the exponent is in the range 4–5. For deformable droplet and bubbles we would expect a smaller index and less hindered settling effect compared to solids, and we adopted $n = 3.5$ that also lead to good fits to the measured profiles. With the addition of gas bubbles, it is natural to expect an increased hindrance effect due to drop/bubble interaction as well as droplet self-interaction.

For a dispersion of type i (oil, water droplets or gas bubbles) we invoke the following generalized model for the hindered settling velocity

$$v_s(\varphi_i,\varphi_a) = V_{\infty,i}\left[1-\left(p\varphi_i + q\varphi_a\right)\right]^n, \tag{9}$$

where φ_a is the "added dispersion" volume fraction in the background mixture that contributes with extra hindrance. The parameters q and p depend on the dispersion types and were tuned to 1.0 for droplets and 0.53 for bubbles. For example, if φ_a is bubbles, then $q = 0.53$, and if φ_a is droplets, then $q = 1.0$. The same property holds for p, with respect to dispersion type φ_i. The smaller parameter value for bubbles may indicate that these have a smaller effect on the hindrance effect due to higher deformation than droplets. Experimental data for hindered settling with effects of bubbles would have been very useful to constrain these parameters.

2.3.3. Buoyancy correction due to gas bubbles

The settling velocity $V_{\infty,i}$ is controlled by buoyancy via the density difference $\Delta\rho$ between the droplet and the background fluid. When the background fluid is a mixture between gas bubbles and fluid, the average background density is reduced, and hence the settling/creaming rate of droplets is increased/reduced. The presence of gas bubbles will then reduce the effective thickness of the dispersion layer of water droplets (steeper density profile) and expand the layer of oil droplets in water (less steep density profile). This affects the average volume fractions in each layer accordingly, and influences the transport rates of droplets along the pipe. The buoyancy effect is less significant for gas bubbles since the background mixture is then composed of fluid droplets and a continuous fluid with small density contrast (between oil and water).

The vertical pressure difference over a droplet is the cause of the buoyancy force. The pressure gradient in the vertical direction is given in terms of the mixture density of the dispersion, $dP/dy = -g\rho_{mix}$, where the generalized mixture density is

$$\rho_{mix} = \rho_c\varphi_c + \rho_a\varphi_a + \rho_i\varphi_i, \tag{10}$$

in terms of the continuous phase and the two dispersed phases. The density difference between the bubble/droplet and the mixed background,

$$\Delta\rho = \rho_i - \rho_{mix}, \tag{11}$$

is to be used in the expression for the settling velocity (4), and ρ in (4) must be replaced by ρ_{mix}. The most general form for the settling velocity, including hindrance, then depends on all dispersion volume fractions,

$$v_s(\varphi_c,\varphi_a,\varphi_i) = V_{\infty,i}(\varphi_c,\varphi_a,\varphi_i)\left[1-\left(p\varphi_i + q\varphi_a\right)\right]^n. \tag{12}$$

With respect to the hindered settling velocity, it is noted that Richardson and Zaki (1954) defined the buoyancy via $\rho_i - \rho_c$ and the value of their index n depends on this definition. Since we use the more general mixture density instead of ρ_c, the corresponding value of the index is larger than the original definition by Richardson and Zaki (1954).

2.4. Turbulent diffusivity with turbulence modification

The magnitude of the turbulent diffusion of the droplets and bubbles responds to the turbulence level. For a relatively large dispersion volume fraction (of bubbles and/or droplets), the turbulence level is reduced relative to a corresponding single phase flow in the same geometry (Skartlien et al., 2023). Hence, diffusion coefficients that are based on single phase arguments will have to be corrected, with a magnitude reduction.

Turbulent diffusion counteracts settling or drift in any direction due to a net diffusion flux away from regions of higher dispersion density. To first order, the diffusivity Γ is based on the characteristic eddy diffusion coefficient

$$\Gamma = 0.07 u_i^* h_i, \tag{13}$$

where the layer height is h_i and the characteristic value of the friction velocity (characteristic velocity fluctuation) in layer i is approximately $u_i^* \simeq \sqrt{2k_i}$ with k_i the average turbulent kinetic energy (per mass unit), including the effect of dispersions. The friction velocity can be estimated by

$$u_{i,0}^* = \sqrt{\frac{\tau_{\text{layer}}}{\rho}} = \sqrt{\frac{\frac{\lambda_{\text{layer}}}{8}\rho U_{\text{layer}}^2}{\rho}}, \tag{14}$$

where λ_{layer} is the Darcy friction factor for the layer. This friction velocity estimate is given only in terms of the total wall and interfacial stresses in the layer, τ_{layer}. These stresses are often evaluated by assuming single phase flow in the layers. An effect that may be important is that turbulent kinetic energy is transported from the faster moving gas layer and down to the liquid layers (Biberg, 2007). The turbulent kinetic energy is then first deposited in the oil layer and then in the water layer, and the characteristic velocity fluctuation in the layers may then be enhanced relative to the local estimate (14). Interfacial waves may also enhance the turbulence level in the liquid by inducing larger scale perturbations well into the layers. If the layer height is relatively thin, the average turbulent kinetic energy in that layer may be affected more by interfacial waves.

Due to these complexities, we introduce a tuning factor f_t for the friction velocities, with the redefinition

$$u_{i,0}^* = f_t \sqrt{\frac{\tau_{\text{layer}}}{\rho}}. \tag{15}$$

We found that the tuned f_t is in the range 0.75–2.3 for the cases we studied, with average values in both layers above unity. With a dispersion profile, we assumed that the local velocity fluctuation is the friction velocity in the layer (15) weighed according to the turbulence suppression induced by the local dispersion volume fraction of gas bubbles and droplets. The model for the turbulence modulation is given below.

When the layer height h_i in (13) is much smaller than the layer width, it is the layer height that is the most important for determining the length scale for the diffusivity. The formally correct length scale would be the half height $h_i/2$ to comply to channel flow. The hydraulic radius $R_{\text{H,i}} = 2A_i/S_i$ where S_i is the wetted perimeter would be more relevant for thicker layers, and in the limit of a filled pipe we would replace the length scale in question with the pipe radius with the classical value of the eddy diffusivity $0.07Ru^*$. In the current work, we used the half height $h_i/2$ for both oil and water layers. The water layer was relatively thin (up to a fraction 0.35 of the pipe diameter), filling the chord segment at the bottom of the pipe, and the overlying water layer was even thinner (up to a fraction 0.2 of the pipe diameter).

The level of the turbulent kinetic energy is determined by the balance between dissipation, energy input from vortex shedding, turbulence production due to the large scale velocity shear and the work performed on the fluid by droplets and bubbles. Skartlien et al. (2023) found that the turbulence modulation in layer i is given approximately by

$$\frac{k_i}{k_0} \simeq \frac{l_h}{l}\left[1 - \varphi_i(1 - \alpha\frac{\rho_p}{\rho_f})\right], \tag{16}$$

if the particle Reynolds number is small so that vortex shedding can be ignored. Here, k_0 is the single phase unmodified value in the layer, φ_i is the average volume fraction of droplets or bubbles in the layer, ρ_p is the droplet or bubble mass density, ρ_f is the continuous fluid mass density, and α is the added mass parameter, defined below. The turbulence length scale (integral length scale) l is the average turbulence length scale and $l_h < l$ is the "hybrid" length scale given by Kenning and Crowe (1997)

$$\frac{1}{l_h} = \frac{1}{\lambda_s} + \frac{1}{l}, \tag{17}$$

where the mean separation between spherical particles in a continuous fluid is

$$\lambda_s = \overline{d}\left(\frac{\pi}{6\varphi_i}\right)^{1/3}, \tag{18}$$

and where $\overline{d}$ is the mean particle diameter. For a volume fraction of about 0.5 of 1 mm diameter bubbles or droplets, λ_s is about 1 mm.

Smaller particle separation enhances dissipation and suppresses the turbulence. The physical interpretation is that enhanced local velocity gradients between the particles increases the viscous dissipation rate. The harmonic mean gives more weight to the separation length scale λ_s if this is smaller than l, and dissipation will be enhanced relative to a single phase fluid. It must be noted that droplet and bubble deformation may result in increased mean separation as these particles are not rigid so that the fluid in the interstitial distance between two passing particles may be slightly larger. Based on single phase flow, the turbulence length scale l takes the form $l = ch_i Re_{layer}^{-1/8}$, where h_i is the layer height, and Re_{layer} is the Reynolds number of the layer. We found that $c = 0.4$ produced a reasonable magnitude of the turbulence suppression k_i/k_0 in the range 0.3–0.6.

The added mass parameter is

$$\alpha = \frac{\frac{3}{2}\frac{\rho_f}{\rho_p}}{1 + \frac{1}{2}\frac{\rho_f}{\rho_p}}, \tag{19}$$

and is in the range $[0, 3]$ from high density to low density particles (solids, via droplets to bubbles). This parameter emerges as the forcing on the particles is due to fluid acceleration via the "added mass effect", in addition to the drag force and other forces (Skartlien et al., 2009). The density ratio ρ_p/ρ_f may be close to unity for droplets in fluid, with $\alpha \simeq 1$. Hence, for droplets with negligible density contrast, one obtains the limit

$$\frac{k_i}{k_0} \simeq \frac{l_h}{l}. \tag{20}$$

The volume fraction of droplets now enters only in of λ_s and therefore in l_h. For bubbles with negligible mass density, one obtains the limit

$$\frac{k_i}{k_0} \simeq \frac{l_h}{l}\left[1 - \varphi_g\right]. \tag{21}$$

The turbulence modulation for droplets and bubbles are therefore very similar for low volume fractions with the ratio l_h/l controlling the level of turbulence modulation. It is seen that this ratio is always less than unity, which implies turbulence suppression. It is confirmed that for sufficiently small volume fraction and large $\lambda_s \gg l$, $l_h \simeq l$, and the turbulence modulation vanishes, so that $k_i = k_0$.

In the three phase model, we adopted the generalized form

$$u_i^* \simeq \sqrt{2k_i} = u_{i,0}^* \sqrt{\frac{l_h}{l}\left[1 - \varphi_i(1 - \alpha\frac{\rho_p}{\rho_f})\right]}, \tag{22}$$

for a single dispersion type in a continuous fluid, where $u^*_{i,0}$ is the friction velocity (15). For a mixture of bubbles and droplets we adopted the plausible extension

$$u_i^* \simeq u_{i,0}^* \sqrt{\frac{\overline{\lambda_s}}{(l+\overline{\lambda_s})}\left[1-\varphi_g(1-\alpha_g\frac{\rho_g}{\rho_f})-\varphi_i(1-\alpha\frac{\rho_p}{\rho_f})\right]}, \tag{23}$$

where the mean separation in the mixture was estimated by

$$\overline{\lambda_s} = \overline{D}\left(\frac{\pi}{6(\varphi_g+\varphi_i)}\right)^{1/3}, \tag{24}$$

and where φ_g is the volume fraction of bubbles in layer i, and $\overline{D}$ is the mean size averaged over both droplets and bubbles,

$$\overline{D} = \frac{\varphi_g \overline{d}_{bubble} + \varphi_i \overline{d}_{droplet}}{\varphi_g+\varphi_i}. \tag{25}$$

Again, experimental data is lacking for turbulence modulation in dispersions in similar settings, even without gas bubbles. The challenge is that the dispersion is generated spontaneously once the required oil and water velocities for emulsification is satisfied. Hence, it may be difficult to obtain dispersion-free reference cases with similar flow rates to record unmodified turbulence levels. The original derivation of Skartlien et al. (2023) governed the average value of the turbulence kinetic energy for the layer as a whole, by considering the influence of a homogeneous dispersion of a single type (either droplets or bubbles). In the current model, we treated the turbulence modulation locally, with the local volume fractions controlling the local value of the turbulent kinetic energy $k_i(y)$, rendering it a function of the vertical coordinate y.

2.5. Dispersion boundary conditions at the large scale interfaces

The large scale interfaces are sources of drops or bubbles; droplets are generated at the oil/water (O/W) interface and bubbles are generated at the gas/oil (G/O) interface (assuming the oil is lighter than water). The current model requires dispersion volume fraction values at the large scale interfaces at specific interfacial heights in the cross section. The average position of the G/O and O/W interfaces cannot be derived directly from the X-ray profiles of the gas, oil or water phases since these profiles are very smooth through the interfacial region due to waves and turbulent fluctuations. We therefore estimated the average interface positions from the data, based on expected dispersion volume fractions there. The model also enforces continuous dispersion profiles through the O/W interface (Fig. 1), according to the measured volume fraction profiles. The implications of this choice is elaborated further in the Discussion section.

The volume fraction of gas bubbles just below the G/O interface, $\varphi_{g,0}$, is uncertain. One choice is the maximum random packing fraction of 0.64 corresponding to random close packing (RCP) of spheres. The actual amount of bubbles will depend on the interfacial dynamics, bubble deformation, and the amount of surface active ingredients in the oil. The random packing fraction governs spheres, while the gas bubbles in the flow may well be highly distorted and even filamentary. For a foam, the gas contents can be much higher than the random packing fraction. To this end we set the boundary value to the RCP value of $\varphi_{g,0} = 0.64$ and define the position of the gas/liquid interface where the measured gas profile volume fraction matches 0.64. The interface position would have been higher up in the cross section for larger $\varphi_{g,0}$, but with little consequence for the model results with respect to profile matching over the full extent of the liquid layers.

The maximum volume fraction of water droplets at the O/W interface could be defined in terms of the inversion point φ_{inv} in a static emulsion, where larger volume fraction of water droplets than φ_{inv} induces a transition from an oil continuous to a water continuous emulsion. However, the inversion point depends on surfactant contents and type, but also the level of turbulent kinetic energy (Salager et al., 2004). Increased turbulence energy shifts the inversion point towards higher values than for a static emulsion, and a water-in-oil emulsion can be maintained at larger water fraction than a smaller static value. Consequently, both the flow rate and surfactant contents in the oil may influence the inversion point. We therefore considered φ_{inv} as a variable parameter, and restricted it to the range 0.4–0.55. The value of φ_{inv} (Table 2) had to be adjusted together with the position of the oil/water interface to obtain a good match to the dispersion profiles. It must be noted that the resulting interface position is restricted to a relatively small height interval, in order to match the measured water profile. It must also be noted that the water volume fraction at the oil/water interface position is smaller than φ_{inv} due to the presence of gas.

The surface area of the O/W LSI is partially occupied by gas bubbles, and the amount of water to be entrained is reduced accordingly. It is assumed that the liquid droplet concentration at the interface is constrained by the gas bubbles, and not be the other way around (that the bubble concentration is constrained by the droplets). The boundary value for the volume fraction of water droplets was therefore taken as

$$\varphi_{w,0} = \varphi_{inv}(1 - b\varphi_{g,o/w}), \tag{26}$$

where $\varphi_{g,o/w}$ is the volume fraction of gas bubbles at the O/W LSI (Fig. 1). The area fraction of oil/water emulsion available for entrainment of water droplets into the oil layer is $(1 - b\varphi_{g,o/w})$. The volume fraction of gas bubbles at the interface can be taken from the calculated gas bubble profile, given the boundary condition $\varphi_{g,0}$ at the G/O interface above. The amount of gas bubbles at the interface may be substantial so that the volume fraction of liquid at the O/W LSI is reduced accordingly, and the water volume fraction there will be far less than the inversion point value.

The tuning factor $b \in [0, 1]$ expresses the fact that the bubble shape may deviate from spheres, with a reduction of the area that is occupied by the bubbles. In the current work we adopted the best tuned value $b = 1$, representing near spherical bubbles. Experimental data is lacking for the morphology for both gas bubbles and droplets at the O/W LSI, and this would require 3D "tomographic" information. 2D projections in video recordings and images are less useful for dense dispersions.

To have a continuous transition of the volume fractions over the O/W interface, it follows that the boundary value of the volume fraction of oil droplets in the underlying water layer must be

$$\varphi_{o,0} = 1 - \varphi_{w,0} - \varphi_{g,o/w} = 1 - \varphi_{g,o/w} - \varphi_{inv}(1 - b\varphi_{g,o/w}). \tag{27}$$

The latter is $(1-\varphi_{inv})(1-\varphi_{g,o/w})$ for $b = 1$, recovering a symmetric form with the water drop boundary condition (26). Here, $1 - \varphi_{inv}$ is the oil volume fraction at the inversion point in the absence of gas.

3. X-ray measurements of dispersion profiles

The experimental data was generated in the high pressure crude oil/natural gas multiphase flow loop at Equinor's Research Centre in Porsgrunn, Norway. This loop was described by Robole et al. (2006), and the datasets will be presented in more detail in a forthcoming publication by Johnson et al. (2024). The system pressure and temperature were 100 bar and 70 °C and the gas density was 68 kg/m^3. The crude oil was obtained from a Brazilian deep water oil field, and the gas phase was natural gas. It should be noted that the crude oil is completely opaque such that visual observation of droplets or bubbles in the oil was not possible. Furthermore, the crude oil has relatively low viscosity at this temperature, only about twice the value of water. The water phase was brine with a salinity matching the field conditions. The key parameters of the fluid system is listed in Table 1. The pipe inclination for the presented cases was one degree relative to the horizontal. The inner pipe diameter is 7.79 cm, while the inner wall roughness was 10 micrometer. An overview of the Equinor Porsgrunn multiphase flow loop infrastructure is shown in Fig. 2. The X-ray tomograph is of the single projection type, with the radiation path directed horizontally as shown in Fig. 3. The single projection type is adequate for stratified flow geometry, and the phases can be separated

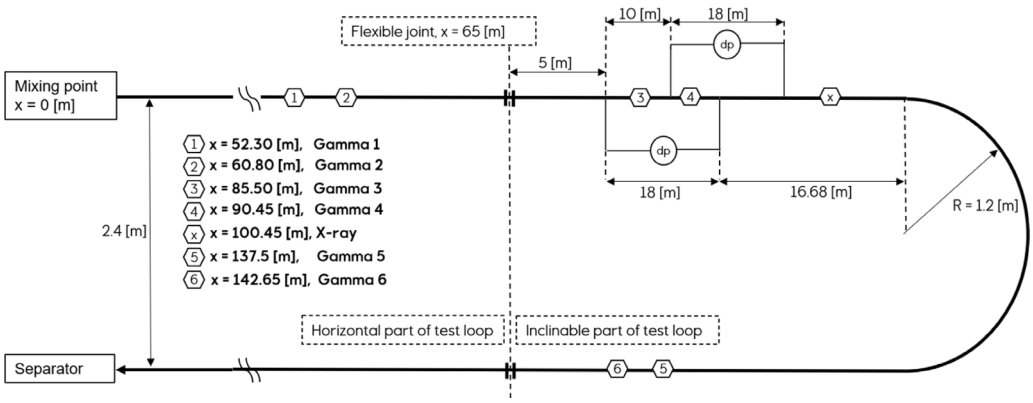

Fig. 2. The Equinor Porsgrunn multiphase flow loop key dimensions including locations of the instrumentation.

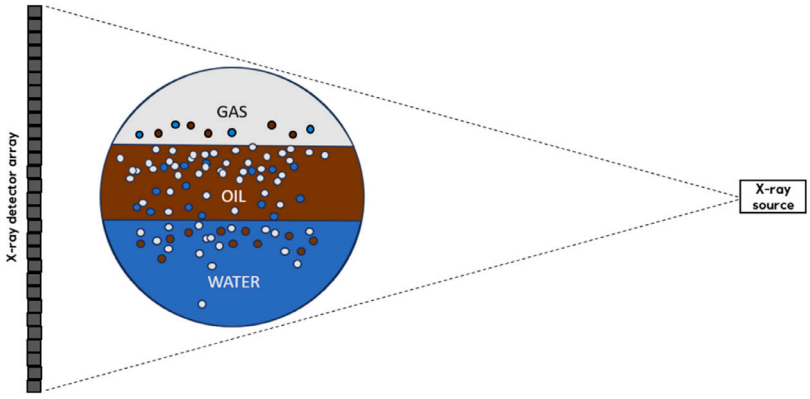

Fig. 3. The side projection X-ray tomograph.

Table 1
Material parameters at 100 bar and 70 degrees Celsius. IFT is interfacial tension.

Water visc.	Oil visc.	Water dens.	Oil dens.	Gas dens.	Gas/oil IFT	Gas/water IFT	Water/oil IFT
0.63 mNs/m^2	1.27 mNs/m^2	1080 kg/m^3	778 kg/m^3	68 kg/m^3	9.5 mN/m	31.2 mN/m	14.2 mN/m

based on the different X-ray attenuation coefficients and with the use of different X-ray energies (“soft band” and “hard band”) (Hu et al., 2005).

It is the time averaged volume fraction profiles we model. The uncertainties in these depend mainly on the physical fluctuations in the flow (turbulence and droplet motion, and interfacial fluctuations) and the corresponding RMS values of the local volume fraction are relatively large as can be seen in the rightmost panel in Fig. 4. In contrast, the statistical measurement errors in the X-ray instrument are much smaller; about 1%–2% in most of the pipe cross section, and on the order of 5% near the pipe walls (Skartlien et al., 2014). The uncertainty in the time average is reduced by a factor $1/\sqrt{N}$ where N is the number of profiles (single snapshots in time) that are averaged over. A sampling rate of 40 Hz was used over a recording interval of 60 s, generating $N \sim 2400$ profiles, such that the uncertainty in the time average is about 0.02 times the local RMS value due to flow fluctuations, which is sufficient accuracy for model development.

The spatial resolution limit in the volume fraction profiles is estimated to be around 2 mm (or about 2.5% of the pipe diameter) based on (Hu et al., 2005) for a similar detector configuration. The corresponding smoothing effect does not introduce significant errors, since it is unlikely that the time averaged volume fraction profile contains gradients on this length scale (and smaller). The contribution to the volume fraction from droplets that are smaller than this resolution limit are registered in terms of the total X-ray opacity of the mix between the continuous and dispersed phases, and reliable estimates of the dispersed phase volume fraction are still achieved. As the X-rays penetrate the droplets, it is the total amount of droplets along the line of sight that matters for the recorded volume fractions (hence it does not matter if several droplets are located along the same line of sight).

The X-ray instrument was located at the end of the test section together with other central instrumentation such as pressure drop, absolute pressure and temperature gauges. This location ensures fully developed stationary flow conditions. The detector pixels were binned into 30 equal partitions in the vertical plane as shown in Fig. 3, and the local phase fractions were recorded over these partitions at a rate of 40 Hz. The corresponding gas, oil and water dispersion profiles were averaged over time (Fig. 4, left panel).

Four cases of double layered dispersion flow were utilized in the modelling, with input parameters to the profile model given in Table 2. These cases have relatively low gas velocity to generate well defined gas, oil and water layers, with dispersions in all three layers, and with gas bubbles mixed into the oil and water layers. Profiles for the averaged volume fraction, and the corresponding standard deviations of the fluctuations, are shown in Fig. 4 for one of the cases. The volume fraction for oil (brown), water (blue), and gas (black) are shown throughout the full cross section of the pipe. The thin black line shows the water fraction in the liquid, $f_w = \varphi_w/(\varphi_w+\varphi_o)$. where values below 0.4–0.5 indicates an oil continuous layer up to the gas/oil interface (marked by the upper horizontal line), and values above indicate a water continuous layer towards the bottom wall.

The standard deviation (RMS fluctuations in time) of the volume fraction was typically 10%–30% for oil and water volume fractions and

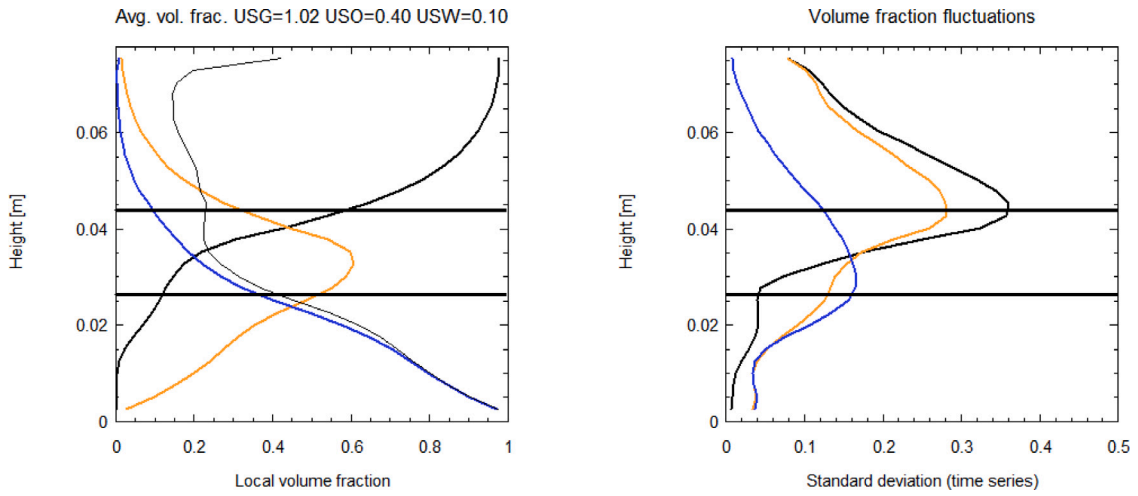

Fig. 4. Data for Case 1, as a typical example. Left: Time averaged volume fraction data as derived from the X-ray instrument with oil (brown lines), water (blue lines), and gas (black lines). The thin black line is the water fraction of the liquid layers (water and oil), and in the gas layer it is the fraction of water droplets relative to both water and oil droplets. The horizontal lines mark the estimated interface locations. Right: The standard deviation in time of the volume fraction, relative to the average volume fraction. The fluctuations were up to 35% near the gas/oil interface, indicating small waves there.

Table 2
Input parameters for the four chosen cases with double layered dispersion flow. The first three columns show the superficial layer phase velocities. The water droplet fractions ϕ_{inv} at the O/W LSI were adjusted to obtain best fits to the profile data. The average droplet and bubble sizes also given (after tuning with f_d from Table 3). The last two columns show the turbulence tuning parameters f_t for the oil and water layers, reflecting the deviation from the local estimate of the friction velocity due to waves and turbulence transport.

CASE	U_{SG} m/s	U_{SO} m/s	U_{SW} m/s	ϕ_{inv}	$\phi_{g,0}$	d_o mm	d_w mm	d_{go} mm	d_{gw} mm	f_t o-layer	f_t w-layer
1	1.02	0.40	0.10	0.40	0.64	0.14	0.36	0.51	0.97	2.30	2.10
2	1.50	0.35	0.15	0.40	0.64	0.12	0.29	0.41	0.79	1.60	1.60
3	2.08	0.35	0.15	0.51	0.64	0.10	0.23	0.33	0.63	0.80	2.00
4	2.63	0.30	0.20	0.50	0.64	0.09	0.21	0.27	0.53	0.75	1.80

Table 3
Common tuning parameters (same for all cases) expressing deviation from the Hinze-estimate of the mean droplet and bubble sizes, hindered settling factors (p for the primary dispersion, or q for the added dispersion, and the value 1.0 expresses no droplet deformation), hindered settling index n, interfacial blocking parameter due to bubbles (with 1.0 expressing spherical bubbles), and scaling factor for the integral length scale in fluid layers.

f_d w-drop	f_d o-drop	f_d bubble	p/q bubble	p/q drops	n index	b blocking	c scale
0.25	0.11	0.45	0.53	1.0	3.5	1.0	0.4

up to about 35% for gas bubbles, near the oil/gas interface marked by the upper horizontal line. This is shown in the right hand panel in Fig. 4. The fact that the RMS value of the gas peaks near the gas/oil interface indicates small waves, turbulent interfacial fluctuations, or intermittent entrainment of gas into the oil layer in "bubble clouds" that are often observed in such flows. The volume fraction of oil responds with large fluctuations as well. The water droplet RMS in the oil layer peaks at slightly lower levels which may indicate the same type of dynamics with waves on the oil/water interface (marked by the lower horizontal line) or with intermittent entrainment of water droplets from the water layer below.

4. Results

4.1. Model tuning and input parameters

The *tuning parameters* of the model, given in Table 3, were adjusted to obtain shapes and magnitudes of the three dispersion profiles that were similar to the X-ray profiles. It should be noted that these tuning parameters were the same for all cases studied. The hindered settling exponent was set to $n = 3.5$, and the interfacial blocking factor by gas bubbles was set to $b = 1$ (corresponding to spherical bubbles). The factor c for the integral length scale of the turbulence in the layers was set to 0.4.

The *input parameters* to the profile model were estimated by using an external multiphase flow model that calculates holdup values (not profiles). These parameters were the friction velocity for each layer (no turbulence modulation) and average droplet and bubble sizes from the Hinze model. These values, as obtained from the external model, were only approximate and had to be adjusted to obtain best matches between the profile model and the data. The average droplet sizes were adjusted according to (7), and the values of the factor f_d (common tuning for all cases) are also given in Table 3. The average droplet sizes (oil,water, gas in oil, and gas in water) after this tuning are given in Table 2.

The friction velocities had to be adjusted for each case (via Eq. (15) with the factor f_t). This is reasonable since interfacial waves and transport of turbulence energy from the gas volume into the liquid layers will also influence the turbulence levels, not only wall and interfacial friction (Biberg, 2007). The influence from interfacial waves may also vary from case to case. These aspects are discussed further in Section 5.

ϕ_{inv} was constrained to the range of 0.4–0.55 and the resulting values are given in Table 2. These are consistent with Brauner and Ullmann (2002) that estimated the inversion point in terms of the oil and water density and viscosity ratios, and based on their formula (21.2) with the current parameters, we found $\phi_{inv} \simeq 0.48$. The full profile of the water fraction f_w in the liquid is shown by the thin black line in the right panel of Fig. 4 for one of the cases, and the value of

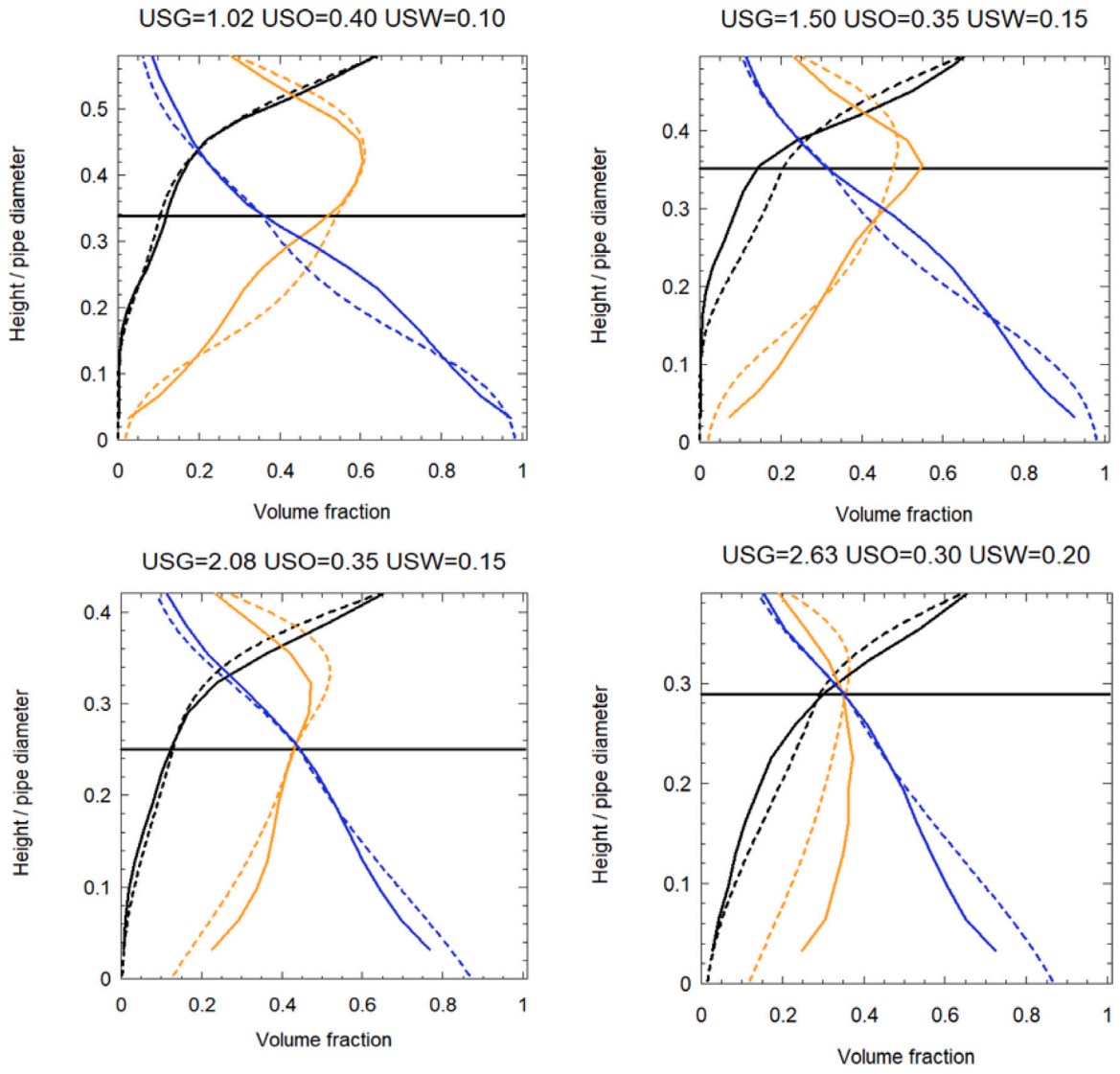

Fig. 5. Results for all four cases. The dashed lines are for the model, with oil (brown lines), water (blue lines), and gas (black lines). The solid lines are time averaged data as derived from the X-ray instrument. Only the modelling domain, up to the gas/oil interface, is shown. The horizontal line marks the estimated location of the oil/water interface.

f_w at the O/W interface is consistent with the adopted value of ϕ_{inv}. It should be noted that the apparent volume fraction at the interface, as recorded by the X-ray instrument, may well be affected by wave fluctuations. The adopted (or tuned) water volume fraction ϕ_{inv} at the interface may therefore deviate with respect to the actual value in the oil continuous phase in the interfacial region.

4.2. Results for double-layered dispersion flow

The model results are shown in Fig. 5. It is clear that the profiles (dashed lines) are qualitatively similar to the data (solid lines). The dispersion profiles are far from simple exponentials due to hindered settling, altered buoyancy and turbulence modulation. Exponential profiles would only occur if the diffusivities and settling velocities were constants, and this is not possible when the phases couple through these mechanisms.

The presence of bubbles results in reduced buoyancy (increased settling effect) in general. The oil droplet profile (brown) then extends further into the water layer and the water droplet profile (blue) steepens, with less water droplets in the overlying oil layer. However, these pure buoyancy effects may be partially masked by turbulence modulation (*e.g.*, less water droplets, more turbulence, less steep profile and vice versa).

Turbulence suppression is due to both bubbles and droplets. Without turbulence modulation, the profiles would be more flat, with a resulting over-prediction of the amount of droplets in either phase. The turbulence damping is largest in the oil layer due to the larger volume fraction of bubbles there. Tuning the friction velocity (15) through f_t affects only the overall slope of the profiles, whereas turbulence modulation varies throughout the layers, with increased suppression for increasing local volume fractions of bubbles and droplets. Hence, turbulence modulation also affects the detailed shape of the profiles.

Hindered settling influences the shape of the profiles as well, typically leading to more blunt profiles at either side of the O/W interface and less extended tails further into the continuous fluid layers. Both gas bubbles and droplets contributes significantly to the local hindrance effect.

Interfacial blocking due to bubbles at the O/W LSI is very significant, with up to 30% area blocking in these cases (corresponding to the volume fraction of bubbles at the O/W interface). Hence, the volume fraction of water at the O/W LSI is less than the inversion point value.

4.3. Impacts in the model from bubbles

In this section, we discuss the response of the model to turning off one physical effect at a time. The results are shown in Fig. 6, with Case

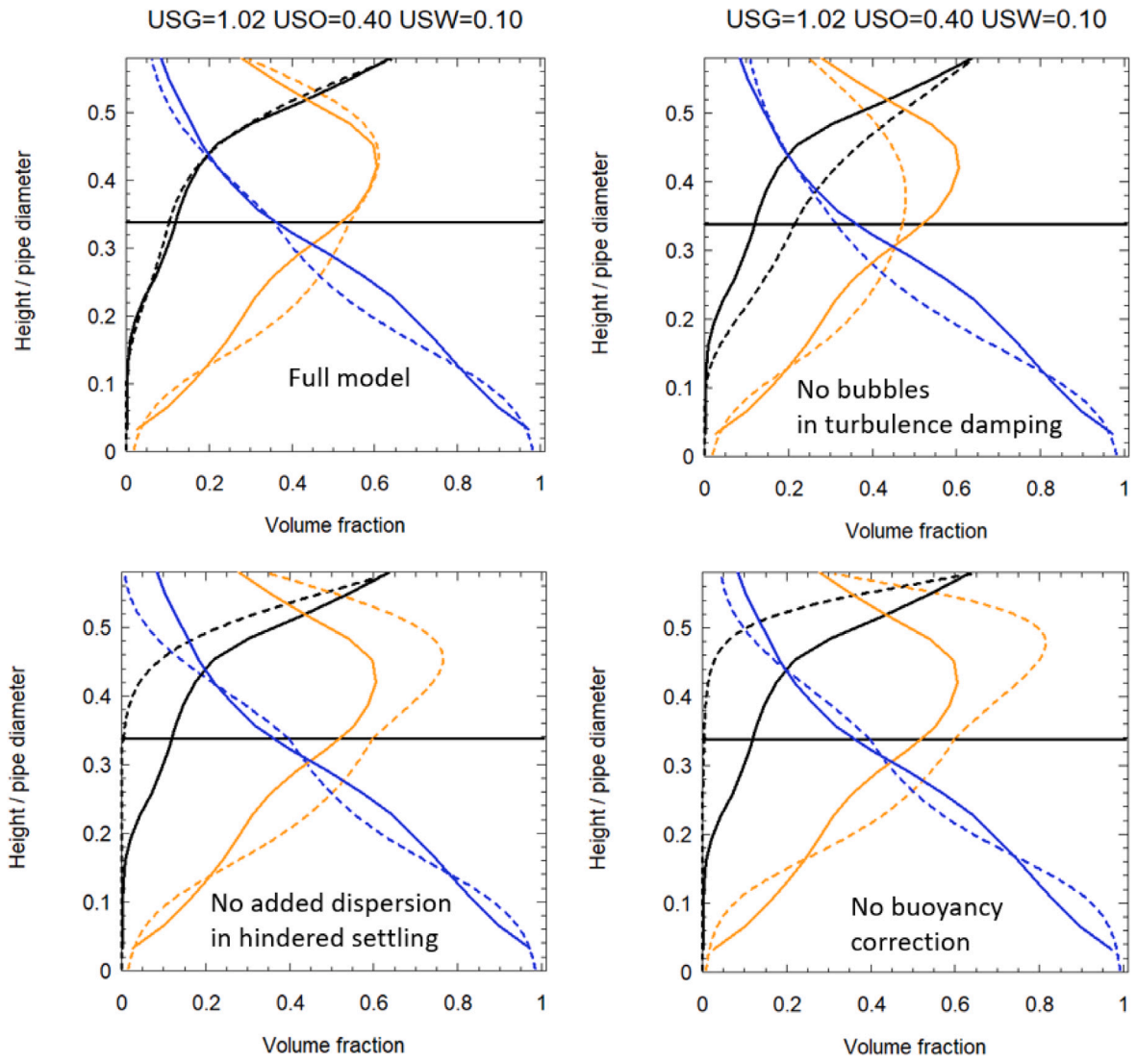

Fig. 6. Various impacts from turning off one physical effect at a time in the model. Upper left: Full model for Case 1. Upper right: Turning off the effect of bubbles in the turbulence modulation. Lower left: Turning off the effect of added dispersion in hindered settling (but keeping the self-induced hindered settling). Lower right: Turning off buoyancy correction in general due to droplets and bubbles. All effects have a significant impact on the profiles.

1 as an example. The upper left panel shows the full model with all effects included, as a reference.

The upper right panel shows the effect from turning off bubbles in the turbulence modulation by setting $\varphi_g = 0$ in Eq. (23),(24),(25). The turbulence level increased and the bubble profile became more flat due to enhanced turbulent diffusion via (13). The elevated bubble fraction in the oil layer reduced the buoyancy of the water droplets there, but the water profile did not become more steep due to a compensating effect of increased turbulence levels.

The lower left panel shows the reduced hindrance effect of turning off the effect of the added dispersion (added droplets for the bubble profile, and added bubbles for the droplet profile) in the hindered settling by setting $\varphi_a = 0$ in (9). The bubble profile became more steep, resulting in almost no bubbles down into the water layer. The buoyancy of the oil droplets in the water layer then increased, and made the oil profile more steep there (the gradient of the brown dashed line in the water layer is now steeper on the average, starting from the interface and proceeding downwards).

The lower right panel shows the effect of turning off the buoyancy correction due to both droplets and bubbles, by setting $\rho_{mix} = \rho_c$ in (10). No buoyancy correction means that the adopted background density is increased, resulting in increased creaming rate of the bubbles. Hence, the bubble profile became much steeper in the oil layer, again leading to almost no droplets in the water layer. Again, this made the oil droplet profile more steep in the water layer (dashed brown line below the interface) since the creaming rate for the oil droplets increased.

4.4. Comparison to a decoupled "classical model"

A more approximate and "classical" way of modelling would be to incorporate hindered settling due to self-interaction only (between bubbles or between droplets), but ignore turbulence modulation and buoyancy effects. This corresponds to a fully decoupled approach where the dispersed phases do not interact. It is therefore interesting to see the difference between no interaction and complete coupling between the phases though the proposed mechanisms.

The left panel in Fig. 7 shows the "classical" approach with hindered settling due to self-interaction only, and no turbulence modulation and buoyancy effects. It is noted that the profiles tend to have the wrong slope. The middle panel shows the result when turbulence modulation is added, which suppresses the turbulence levels so that the oil and water dispersion profiles get more steep and become qualitatively similar to the data. This indicates that turbulence modulation is an important ingredient.

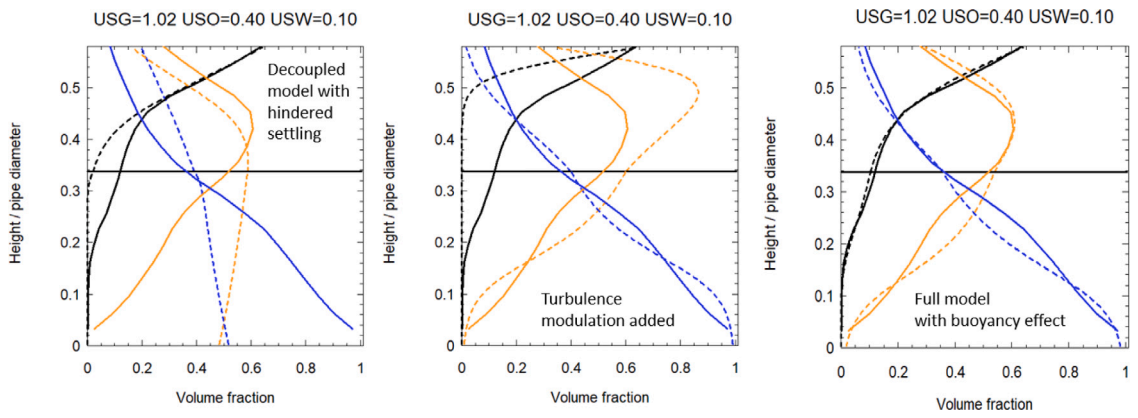

Fig. 7. The left panel shows a decoupled model with hindered settling due to self-interaction only. The dashed lines are for the model and the solid lines are the data. The middle panel shows the result when turbulence modulation is added. The right hand panel shows the full model including altered buoyancy and hindered settling due to both bubbles and droplets.

The right hand panel shows the result when also the buoyancy correction is added, which also brings the gas bubble profile into agreement with the data. The buoyancy effect due to high bubble density has a large impact in the upper parts of the oil layer. The generalized hindered settling model was also included here, recovering the full model.

5. Discussion

The most significant deviations between the profile model and the data appeared to be for the oil droplet profile in the water layer (Fig. 5). A source of deviation may be an inaccurate representation of the turbulence inhomogeneity. Another possible source of deviation is due to interfacial waves that may entrain "bubble clouds" or "droplet clouds" in response to the interfacial dynamics and this may influence both the averaged profiles and the RMS values.

The interfacial boundary conditions were formulated with the constraint of continuity of the volume fraction profile through the interfacial region, in order to match the data. An effect of interfacial waves is the smoothing of the averaged (and measured) volume fraction profile in the transition from the continuous to the dispersed state over the interfacial region. We did not account for this smoothing effect, but rather set the volume fraction at the interface directly. Volume fraction profiles without the presence of waves could in principle be near discontinuous at the interface when the entrainment rate is relatively small, and strictly discontinuous when the entrainment is zero. A model could also be formulated in this way via entrainment relations (rather than the inversion point argument) and the modelled profiles could then be smoothed to account for waves in the interfacial region. This latter approach would be more complex and further uncertainties would be added via that chosen entrainment relations.

A third approach for the formulation of interfacial boundary conditions could be in terms of interfacial energy (gravity, interfacial tension, local curvature and viscous work), including the effect of waves (Skartlien et al., 2014). The position of the interface is then expressed in terms of a probability distribution (PDF), and the volume fraction profile through the interfacial region is formulated in terms of the integral of this PDF.

To obtain good fits to the data, we had to tune the turbulence factors f_t (for the friction velocity given by (15)) for the oil and water layers for each case (the tuned factors are given in Table 2, last two columns). A possible reason for the variation of these tuning factors is an influence of interfacial waves on the G/O and O/W interfaces, and/or turbulent transport from the faster moving gas into the liquid layers. These effects were not accounted for in model for the friction velocity. With these effects, one would expect larger effective turbulence levels in the fluid layers and the resulting tuning factors were in fact larger than 1.0 on the average.

The current model is a good starting point for other cases with different fluids with different densities, viscosities and interfacial tension, but it is likely that the model would need a re-tuning due to the uncertainties in the sub-models used. It must be noted that the model is strictly valid only for statistically stationary plane-parallel stratified flow with a balance between the upward and downward dispersion fluxes. Furthermore, the model cannot be used for higher flow velocities in the transition to annular flow due to the geometry restriction. It is doubtful that the model could be used with high accuracy for slug flow due to the transient nature of both the slug and film regions with local imbalance between upward and downward dispersion fluxes.

In general, the dispersion distribution has an effect on the pressure drop in terms of altering the layer thicknesses and the associated contact area between the continuous fluid and the wall, modifying the effective viscosity of the mixture near the walls, and affecting the turbulence levels relative to a dispersion free fluid.

6. Conclusion

This work developed a three-phase dispersion profile model including the interaction between oil or water droplets and gas bubbles, using well known principles and basic sub-models for the various physical mechanisms for single-type dispersions. These sub models introduced tuning parameters as a consequence of the uncertainties associated to each model in this complex setting of bubbles interacting with droplets. More experimental work would be needed to reduce the uncertainties, primarily with respect to the influence of gas bubbles on droplet sizes, hindered settling and turbulence modulation.

Only the most essential physical mechanisms were incorporated among those that are expected to occur in a three-phase dispersion flow. Despite of the mentioned uncertainties, the shape and magnitude of the measured profile data could be reproduced qualitatively with bubble-related corrections in terms of enhanced hindered settling, droplet buoyancy, and turbulence suppression. Bubbles strongly influence the buoyancy in the oil layer where the bubble fraction is large, and bubbles enhance the hindered settling effect on dispersion droplets. The results indicated that turbulence suppression may be a significant effect, and increased volume fraction locally of gas bubbles and droplets suppresses the turbulence level and leads to steeper dispersion profiles, similar to the measured profiles. Reduced buoyancy due to bubbles expanded the bubble layer more into the oil and water, and the effect on the droplets is more significant in the oil layer where the bubble fraction is larger. The buoyancy effect compressed the dispersion layer of water droplets in the oil and expanded the dispersion layer of oil in the water, if the gas bubble concentration was significant there.

We encourage further experiments to gain more insight into the potential importance of turbulence modulation and hindered settling effects in dispersion flow, also in the presence of gas bubbles. Droplet entrainment and interfacial boundary conditions in three phase flow is also a topic for further experimental studies, as well as droplet size distributions in the presence of gas bubbles. It is suspected that the Hinze model (or similar single-type droplet models) for the average droplet size could be replaced by a better formulation built on a balance between breakup and coalescence in the presence of gas bubbles.

CRediT authorship contribution statement

R. Skartlien: Writing – review & editing, Writing – original draft, Software, Methodology, Investigation, Formal analysis, Conceptualization. **J. Nossen:** Methodology, Data curation, Conceptualization. **G.W. Johnson:** Supervision, Investigation, Data curation. **T.K. Kjeldby:** Writing – review & editing, Project administration, Funding acquisition, Formal analysis, Data curation.

Declaration of competing interest

The authors declare that they have no known competing financial interests or personal relationships that could have appeared to influence the work reported in this paper.

Acknowledgments

The project was financed by Equinor through the Frame Agreement between IFE and Equinor. P.S. Johansson and M. Nordsveen shared insights in many useful discussions. O. Skjæraasen provided information on the separation of the three phases using an X-ray instrument. P.S. Johansson proofread the manuscript at an early stage.

Data availability

Data will be made available on request.

References

Ahmed, S.A., John, B., 2018. Liquid - Liquid horizontal pipe flow - A review. J. Pet. Sci. Eng. 168, 426–447. http://dx.doi.org/10.1016/j.petrol.2018.04.012, URL: https://www.sciencedirect.com/science/article/pii/S0920410518303176.

Amundsen, L., 2011. An Experimental Study of Oil-Water Flow in Horizontal and Inclined Pipes (Ph.D. thesis).

Angeli, P., Hewitt, G., 1999. Pressure gradient in horizontal liquid-liquid flows. Int. J. Multiph. Flow 24 (7), 1183–1203. http://dx.doi.org/10.1016/S0301-9322(98)00006-8, URL: https://www.sciencedirect.com/science/article/pii/S0301932298000068.

Angeli, P., Hewitt, G.F., 2000. Drop size distributions in horizontal oil-water dispersed flows. Chem. Eng. Sci. 55 (16), 3133–3143. http://dx.doi.org/10.1016/S0009-2509(99)00585-0, URL: https://www.sciencedirect.com/science/article/pii/S0009250999005850.

Biberg, D., 2007. A mathematical model for two-phase stratified turbulent duct flow. Multiph. Sci. Technol. 19 (1), 1–48.

Bragg, A.D., Ireland, P.J., Collins, L.R., 2015. On the relationship between the non-local clustering mechanism and preferential concentration. J. Fluid Mech. 780, 327–343. http://dx.doi.org/10.1017/jfm.2015.474.

Bragg, A.D., Richter, D.H., Wang, G., 2021. Mechanisms governing the settling velocities and spatial distributions of inertial particles in wall-bounded turbulence. Phys. Rev. Fluids 6, 064302. http://dx.doi.org/10.1103/PhysRevFluids.6.064302, URL: https://link.aps.org/doi/10.1103/PhysRevFluids.6.064302.

Brauner, N., Ullmann, A., 2002. Modeling of phase inversion phenomenon in two-phase pipe flows. Int. J. Multiph. Flow 28 (7), 1177–1204. http://dx.doi.org/10.1016/S0301-9322(02)00017-4, URL: https://www.sciencedirect.com/science/article/pii/S0301932202000174.

Eaton, J., Fessler, J., 1994. Preferential concentration of particles by turbulence. Int. J. Multiph. Flow 20, 169–209. http://dx.doi.org/10.1016/0301-9322(94)90072-8, URL: https://www.sciencedirect.com/science/article/pii/0301932294900728.

Elseth, G., 2001. An Experimental Study of Oil/Water Flow in Horizontal Pipes (Ph.D. thesis).

Evripidou, N., Avila, C., Angeli, P., 2022. A mechanistic model for the prediction of flow pattern transitions during separation of liquid-liquid pipe flows. Int. J. Multiph. Flow 155, 104172. http://dx.doi.org/10.1016/j.ijmultiphaseflow.2022.104172, URL: https://www.sciencedirect.com/science/article/pii/S0301932222001586.

Feng, Z.-G., Michaelides, E.E., 2001. Drag coefficients of viscous spheres at intermediate and high Reynolds numbers. J. Fluids Eng. 123 (4), 841–849. http://dx.doi.org/10.1115/1.1412458.

Gore, R., Crowe, C., 1989. Effect of particle size on modulating turbulent intensity. Int. J. Multiph. Flow 15 (2), 279–285. http://dx.doi.org/10.1016/0301-9322(89)90076-1, URL: https://www.sciencedirect.com/science/article/pii/0301932289900761.

Hetsroni, G., 1989. Particles-turbulence interaction. Int. J. Multiph. Flow 15 (5), 735–746. http://dx.doi.org/10.1016/0301-9322(89)90037-2, URL: https://www.sciencedirect.com/science/article/pii/0301932289900372.

Hewitt, G., 2005. Three-phase gas-liquid-liquid flows in the steady and transient states. Nucl. Eng. Des. 235 (10), 1303–1316. http://dx.doi.org/10.1016/j.nucengdes.2005.02.023, URL: https://www.sciencedirect.com/science/article/pii/S0029549305001020. Festschrift Edition Celebrating the 65th Birthday of Prof. Richard T. Lahey, Jr.

Hinze, J.O., 1955. Fundamentals of the hydrodynamic mechanism of splitting in dispersion processes. AIChE J. 1 (3), 289–295. http://dx.doi.org/10.1002/aic.690010303, URL: https://aiche.onlinelibrary.wiley.com/doi/abs/10.1002/aic.690010303.

Hu, B., Stewart, C., Hale, C., Lawrence, C., Hall, A., Zwiens, H., Hewitt, G., 2005. Development of an X-ray computed tomography (CT) system with sparse sources: Application to three-phase pipe flow visualization. Exp. Fluids 39, 667–678. http://dx.doi.org/10.1007/s00348-005-1008-2.

Ioannou, K., Nydal, O.J., Angeli, P., 2005. Phase inversion in dispersed liquid-liquid flows. Exp. Therm Fluid Sci. 29 (3), 331–339. http://dx.doi.org/10.1016/j.expthermflusci.2004.05.003, URL: https://www.sciencedirect.com/science/article/pii/S0894177704000615. Third European-Japanese Two-Phase Flow Group Meeting.

Johnson, G., Kjeldby, T., Johansson, P., 2024. Dispersions in three-phase high pressure slug flows based on x-ray data. (in preparation).

Kenning, V., Crowe, C., 1997. On the effect of particles on carrier phase turbulence in gas-particle flows. Int. J. Multiph. Flow 23 (2), 403–408. http://dx.doi.org/10.1016/S0301-9322(96)00070-5, URL: https://www.sciencedirect.com/science/article/pii/S0301932296000705.

Khor, S., 1998. Three-Phase Liquid-Liquid-Gas Stratified Flow in Pipelines (Ph.D. thesis). Imperial College London (University of London).

Kjølaas, J., Schumann, H., Gonzalez, D., Johansen, S.T., 2022. Modelling of dispersed oil/water flow in a near-horizontal pipe. Chem. Eng. Sci. 263, 118074. http://dx.doi.org/10.1016/j.ces.2022.118074, URL: https://www.sciencedirect.com/science/article/pii/S0009250922006583.

Lovick, J., Angeli, P., 2004. Experimental studies on the dual continuous flow pattern in oil-water flows. Int. J. Multiph. Flow 30 (2), 139–157. http://dx.doi.org/10.1016/j.ijmultiphaseflow.2003.11.011, URL: https://www.sciencedirect.com/science/article/pii/S0301932203002180.

Mei, R., 1994. Effect of turbulence on the particle settling velocity in the nonlinear drag range. Int. J. Multiph. Flow 20 (2), 273–284. http://dx.doi.org/10.1016/0301-9322(94)90082-5, URL: https://www.sciencedirect.com/science/article/pii/0301932294900825.

Ngan, K.H., Ioannou, K., Rhyne, L.D., Wang, W., Angeli, P., 2009. A methodology for predicting phase inversion during liquid-liquid dispersed pipeline flow. Chem. Eng. Res. Des. 87 (3), 318–324. http://dx.doi.org/10.1016/j.cherd.2008.09.012, URL: https://www.sciencedirect.com/science/article/pii/S026387620800292X.

Pal, R., Rhodes, E., 1985. A novel viscosity correlation for non-newtonian concentrated emulsions. J. Colloid Interface Sci. 107 (2), 301–307. http://dx.doi.org/10.1016/0021-9797(85)90181-X, URL: https://www.sciencedirect.com/science/article/pii/002197978590181X.

Paolinelli, L.D., 2020. A comprehensive model for stability of dispersed oil-water flow in horizontal and inclined pipes. Chem. Eng. Sci. 211, 115325. http://dx.doi.org/10.1016/j.ces.2019.115325, URL: https://www.sciencedirect.com/science/article/pii/S0009250919308152.

Piela, K., Delfos, R., Ooms, G., Westerweel, J., Oliemans, R., 2008. On the phase inversion process in an oil-water pipe flow. Int. J. Multiph. Flow 34 (7), 665–677. http://dx.doi.org/10.1016/j.ijmultiphaseflow.2007.12.004, URL: https://www.sciencedirect.com/science/article/pii/S0301932208000104.

Reeks, M.W., 2014. Transport, mixing and agglomeration of particles in turbulent flows. J. Phys. Conf. Ser. 530 (1), 012003. http://dx.doi.org/10.1088/1742-6596/530/1/012003.

Richardson, J., Zaki, W., 1954. The sedimentation of a suspension of uniform spheres under conditions of viscous flow. Chem. Eng. Sci. 3 (2), 65–73. http://dx.doi.org/10.1016/0009-2509(54)85015-9, URL: https://www.sciencedirect.com/science/article/pii/0009250954850159.

Robole, B., Kvandal, H.K., Schuller, R.B., 2006. The Norsk Hydro multiphase flow loop: a high pressure flow loop for real three-phase hydrocarbon systems. Flow Meas. Instrum. 17 (3), 163–170. http://dx.doi.org/10.1016/j.flowmeasinst.2006.01.003, URL: https://www.sciencedirect.com/science/article/pii/S0955598606000124. Calibration Facilities.

Saber, A., Lundström, T.S., Hellström, J.G.I., 2015. Turbulent modulation in particulate flow: A review of critical variables. Engineering 07, 597–609.

Sajjadi, S., Zerfa, M., Brooks, B.W., 2002. Dynamic behaviour of drops in oil/water/oil dispersions. Chem. Eng. Sci. 57 (4), 663–675. http://dx.doi.org/10.1016/S0009-2509(01)00415-8, URL: https://www.sciencedirect.com/science/article/pii/S0009250901004158.

Salager, J.-L., Forgiarini, A., Marquez, L., Pena, A., Pizzino, A., Rodriguez, M.P., Rondon-Gonzalez, M., 2004. Using emulsion inversion in industrial processes. Adv. Colloid Interface Sci. 108–109, 259–272. http://dx.doi.org/10.1016/j.cis.2003.10.008, URL: https://www.sciencedirect.com/science/article/pii/S0001868603001544. Emulsions, From Fundamentals to Practical Applications.

Sassi, P., Stiriba, Y., Lobera, J., Palero, V., Pallarés, J., 2020. Experimental analysis of gas-liquid-solid three-phase flows in horizontal pipelines. Flow Turbul. Combust. 1–20, URL: https://api.semanticscholar.org/CorpusID:218960852.

Skartlien, R., 2009. A droplet transport model for channel and pipe flow based on particle kinetic theory and a stress-ω turbulence model. Int. J. Multiph. Flow 35 (7), 603–616. http://dx.doi.org/10.1016/j.ijmultiphaseflow.2009.03.009, URL: https://www.sciencedirect.com/science/article/pii/S0301932209000585.

Skartlien, R., Drazen, D., Swailes, D., Jensen, A., 2009. Suspensions in turbulent liquid pipe flow: Kinetic modelling and added mass effects. Int. J. Multiph. Flow 35 (11), 1017–1035. http://dx.doi.org/10.1016/j.ijmultiphaseflow.2009.07.001, URL: https://www.sciencedirect.com/science/article/pii/S030193220900113X.

Skartlien, R., Grimes, B., Meakin, P., Sjöblom, J., Sollum, E., 2012. Coalescence kinetics in surfactant stabilized emulsions: Evolution equations from direct numerical simulations. J. Chem. Phys. 137 (21), 214701. http://dx.doi.org/10.1063/1.4768243.

Skartlien, R., Hu, B., Palmer, T., Staff, G., Sollum, E., 2014. A statistical model for the average volume fraction profile through the mixing zone in turbulent stratified gasâ€“liquid flow. Int. J. Multiph. Flow 59, 160–172. http://dx.doi.org/10.1016/j.ijmultiphaseflow.2013.11.002, URL: https://www.sciencedirect.com/science/article/pii/S0301932213001870.

Skartlien, R., Palmer, T.L., Skjæraasen, O., 2023. A generalized $k-\epsilon$ model for turbulence modulation in dispersion and suspension flows. Int. J. Multiph. Flow 167, 104549. http://dx.doi.org/10.1016/j.ijmultiphaseflow.2023.104549, URL: https://www.sciencedirect.com/science/article/pii/S0301932223001702.

Skartlien, R., Sollum, E., Schumann, H., 2013. Droplet size distributions in turbulent emulsions: Breakup criteria and surfactant effects from direct numerical simulations. J. Chem. Phys. 139 (17), 174901. http://dx.doi.org/10.1063/1.4827025.

Smith, I.E., Nossen, J., Kjølaas, J., Lund, B., 2015. Development of a steady-state point model for prediction of gas/oil and water/oil pipe flow. J. Dispers. Sci. Technol. 36 (10), 1394–1406. http://dx.doi.org/10.1080/01932691.2014.989568.

Taitel, Y., Barnea, D., Brill, J., 1995. Stratified three phase flow in pipes. Int. J. Multiph. Flow 21 (1), 53–60. http://dx.doi.org/10.1016/0301-9322(94)00058-R, URL: https://www.sciencedirect.com/science/article/pii/030193229400058R.

Valle, A., 2000. Three Phase Gas-Oil-Water Pipe Flow (Ph.D. thesis). Imperial College London (University of London).

Yaqub, M.W., Marappagounder, R., Rusli, R., Prasad, R., Pendyala, R., 2020. Review on gas-liquid-liquid three-phase flow patterns, pressure drop, and liquid holdup in pipelines. Chem. Eng. Res. Des. 159, 505–528. http://dx.doi.org/10.1016/j.cherd.2020.04.029, URL: https://www.sciencedirect.com/science/article/pii/S0263876220301866.